Article

Not peer-reviewed version

Recycled Carbon Black/Hdpe Composite from Waste Tires: Manufacturing, Testing and Aging Characterization

Catherine Billotte , Laurence Romana , Anny Flory , Serge Kaliaguine , Eduardo Ruiz *

Posted Date: 21 August 2024

doi: 10.20944/preprints202408.1560.v1

Keywords: Waste tires, Carbon Black, HDPE, polymer aging

 doi:10.20944/preprints202408.1560.v1

Article

Developing a Recycled Carbon Black/HDPE Composite from Waste Tires: Manufacturing, Testing and Aging Characterization

Catherine Billotte [1], Laurence Romana [2], Anny Flory [2], Serge Kaliaguine [3] and Edu Ruiz [1,*]

[1] Polytechnique Montréal, Département de Génie Mécanique, C.P. 6079, succ. Centre-Ville, Montréal (Québec), H3C 3A7, Canada, Université des Antilles, Groupe de Technologie des Surfaces et Interfaces, Campus de Fouillole, 97159 Pointe à Pitre Cedex, Guadeloupe, French West Indies
[2] Université des Antilles, Groupe de Technologie des Surfaces et Interfaces, Campus de Fouillole, 97159 Pointe à Pitre Cedex, Guadeloupe, French West Indies
[3] Université Laval, Département de Génie Chimique, 1065 avenue de la Médecine, Québec (Québec), G1V 0A6, Canada
* Correspondence: edu.ruiz@polymtl.ca

Abstract: This study addresses the global issue of recycling used vehicle rubbish tires, typically burned out or trimmed to be reused in playground floors or road banks. In this study we explore a novel environmentally responsive approach or decomposing and recovering the carbon black particles contained in tires (25-30 wt.%) by vacuum pyrolysis. Given that carbon black is well known for its UV protection in plastics, the objective of this research is to provide an ecological alternative to commercial carbon black of fossil origin by recycling the carbon black (rCB) from used tires. In our research, we create a composite material using rCB and high density polyethylene (HDPE). In this article we present the environmental aging studies carried out to this composite material. The topographic evolution of the samples with aging and the oxidation kinetic of the surface and through the thickness were studied. A Beer-Lambert law is used to relate the oxidative index to the characteristic depth of the samples. This work helps to demonstrate the feasibility of using recycled carbon black particles from waste tires as a filler for UV protection.

Keywords: HDPE; recycled carbon black; pyrolysis; photooxidation; FTIR; oxygen diffusion; accelerated aging

1. Introduction

Nearly one billion of rubbish tires are manufactured worldwide each year and this is constantly increasing with the society growth, which makes recycling of waste tires a constant challenge [1,2]. Even if recycling by trimming and recovery are performed in many countries, millions of tires are still dumped in large landfills and if improperly managed they may cause rubber pollution. Their accumulation presents significant risks, and the probability of fire is high, conducting to environmental disasters. The life cycle assessment has demonstrated that the most polluting of the tire is not its manufacture but its end of life; a tire contains more than one-hundred raw materials, most of which are not biodegradable [3]. It is therefore fundamental to develop alternatives allowing the recycling and recovery of waste tires with an environmental perspective. In developed countries the recycling industry has adopted granulation (e.g., production of stabs, field turf or rubber fillers) or the use of tires as fuel for their high energy value in combustion/incineration [4–6]. New generations are pushing the legislation towards environmental consciousness, forcing the industry to adopt more recycled products in their manufacturing process [1,7]. Our research project aims at developing new composite materials made out of recycled carbon black from waste tires by a eco-friendly vacuum pyrolysis process [2,8].

 doi:10.20944/preprints202408.1560.v1

Waste tire pyrolysis (see **Figure 1**) is a process of thermal decomposition of organic materials under heat in a controlled non-oxidative condition, leading to three main sub-products: a solid residue, gaseous and liquid hydrocarbons. The hydrocarbon sub-products can be revalorized and the solid residue, so-called the char, can be retreated for its valorization. The pyrolysis char is mainly composed of carbon black and other organic solid materials contained in the tire composition [8,9]. Carbon black (CB) is a common filler used to provide UV protection to polyolefin plastic applications, such as piping, roof membranes, electric cables and wires, geotextiles, and other outdoor products [10–12]. Commercial carbon black is made by thermal decomposition or partial combustion of hydrocarbons such as oil or natural gas. The tire industry is a major end user of carbon black particles. In the USA, tire industry is responsible for 70% of the total production of carbon black [13]. Commercial CB typically used in composite materials manufacturing, generates a carbon footprint of 1.08 kg CO^2/ kg of CB (ecoinvent v3.6 database [14]). The substitution of newly produced CB by rCB from waste tire pyrolysis reduced the carbon footprint to 0.43 kg CO^2/ kg CB [14]. The pyrolysis recycling of CB therefore makes it possible to reduce carbon footprint by 60% while being at competitive price.

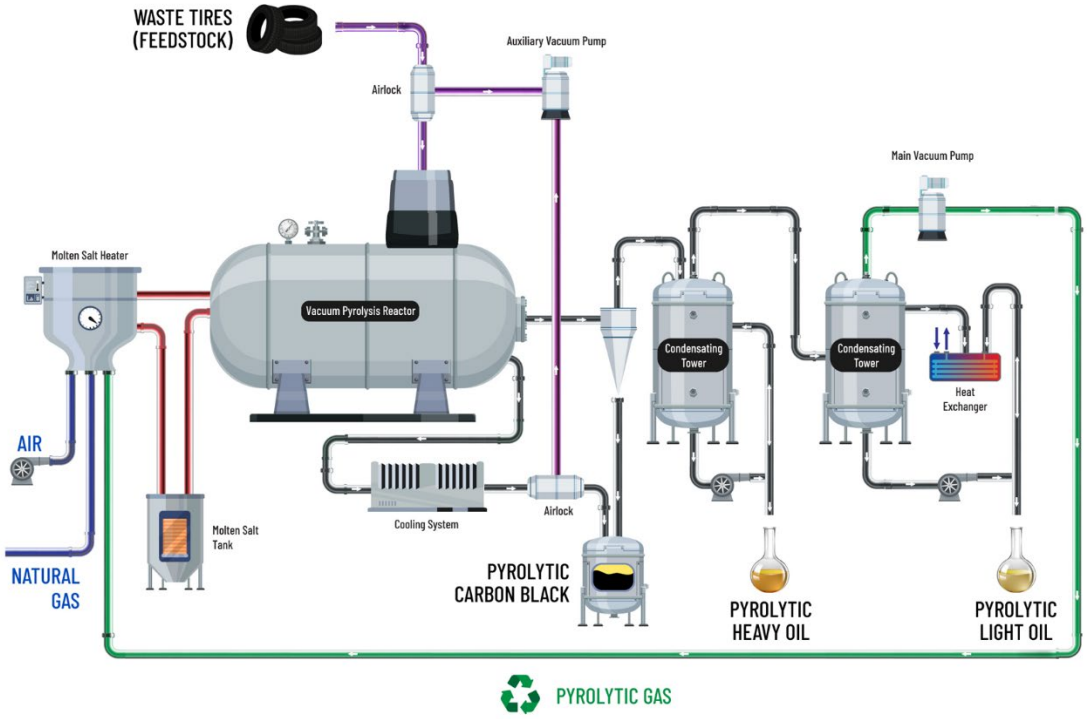

Figure 1. Vacuum pyrolysis process of Pyrovac Inc.

Furthermore, the commercial value of the recycled carbon black is increasing as recycling processes are being developed and optimized to produce good quality particles at high rates. The ability to replace commercial carbon black by recycled solutions, is directly related to capability of the pyrolysis process of waste tires [3,15]. The quality and consistency of pyrolytic recycled carbon black can vary significantly; in particular because it contains various different carbon black grades used into the tire composition and because of the diversity of tires in the recycling process (from cars, trucks, tractors, bikes, etc.). This high variability of mixed tires and particles makes it difficult to optimize the pyrolysis processing conditions to aim recovering a certain grade of carbon black particles for a specific use [16]. In addition, the pyrolytic carbon black contains a portion of ash (12-17 wt.%) and carbonaceous deposits on the surface of the particles [9,17], making the particles smoother. These deposits have a detrimental impact on the surface area of the particles and on their ability to bond, and therefore reduce their performance in reinforcing plastics and elastomers [18,19]. Carbonaceous deposits are the result of thermal cracking due to an accumulation of the volatiles during tire decomposition, which has the effect of clogging the pores of the particle. The vacuum

 doi:10.20944/preprints202408.1560.v1

pyrolysis process of Pyrovac Inc. makes it possible to limit these side reactions because the volatiles hydrocarbons are constantly evacuated by the vacuum pressure [9]. Pyrolytic carbon black thus has surface properties that are closer to those of commercial carbon black used in the composition of tires [18].

Plastic materials exposed to direct sun light radiation conditions such as in tropical climate, require a tailored UV protection and anti-oxidant capability for long term durability. Typical sunlight radiation in tropical areas is characterized by high temperatures (annual average of +26°C), high relative humidity (annual average of 70-80%) and solar irradiation of more than 200 KWh/m^2 [20,21]. These environmental conditions are the primary cause of polymer degradation, having a significant impact on their durability [20]. Polyolefins are the most used polymers in industry and are sensitive to UV radiation and temperature, which affects their mechanical performance over time. The degradation mechanism of polyolefins has been extensively studied by researchers [21–24], it starts with a photolysis reaction of one of the chromophores present in the polymer leading to the formation of free radicals which react with the polymer chains in the presence of oxygen. Oxidation products are then formed according to a loop mechanism [21,25]. Chemical aging affects the molecular structure of the polymer, mainly with chain scissions and crosslinking, having an impact on mechanical properties and on the surface aesthetic of the polymer (discoloration). To improve their durability, a typical approach consists in mixing the polymer with solid particles to act as a filter to sun rays is often used. Carbon black is a material known for its sun radiation absorption performance, it acts as a radical scavenger, a radical trap or UV absorber [11,12,26,27]. It should be noted however that it can also have the opposite effect, acting as a pro-oxidant, as reported by Horrocks et al. for polypropylene composite tapes made with carbon black [12]. This would be due to the concentration of oxygenated groups on the surface of the carbon black particles, which would adsorb the antioxidants present in the polymer or by thermo-oxidative reactions on the surface of the particles, the carbon black acting as a catalyst in the peroxide decomposition and the formation of the free radicals, enhancing the oxidation process. The surface of carbon black particles has to be treated to reduce oxygenated groups and to grasp functional groups for better adhesion to the polymer.

In this work the recycled carbon black (rCB) from vacuum pyrolysis of waste tires was used as UV protection filler in a high density polyethylene (HDPE) matrix. To study the protection performance of recycled carbon black, HDPE samples with and without recycled carbon black were aged under accelerated conditions. FTIR spectroscopy was used to detect the change in sample oxidation over time and the surface topography of the samples was studied by optical microscopy. The amount of oxidation products as a function of the sample thickness was also evaluated on pure HDPE and HDPE containing rCB. The depth oxidation distribution profiles were fitted using a Beer-Lambert law. The antioxidant action of the recycled carbon black is finally discussed.

2. Experimental

2.1. Materials

The recycled carbon black (rCB) used is supplied by Pyrovac Inc. It was obtained by vacuum pyrolysis (530°C, 15-20 kPa) of waste tires and comes from a demonstration industrial plant of 540 kg/h located at Ville de Saguenay (Québec, Canada) and has received no post-treatment. The tire recycling process is reported in Roy et al. [9]. The rCB used in this work [9] has a surface of 77.3 m^2/g (multipoint nitrogen surface area), a structure of 95 cm^3/100 g (oil absorption number) and a ash content of 15.7 wt.% [9].

High density polyethylene from Dow Chemicals (HDPE Dow™ DMDA-8904 NT 7) was used in this study as the plastic resin. This material is largely used in outdoor plastic applications, and in particular in piping, which allows a possible application for the irrigation of crops in the agricultural field in tropical climate such as Guadeloupe (FWI). It has a melt index of 4.4 g/ 10 min and a density at room temperature of 0.952 kg/m^3 [28]. The choice of using a petroleum (and non-recycled) HDPE matrix was made in order to limit the only variability related to recycling to the carbon black particles.

2.2. Sample Preparation

 doi:10.20944/preprints202408.1560.v1

Figure 2 shows the steps carried out in this work during the preparation of the HDPE/rCB composite materials. The average size of rCB particles at the exit of the pyrolysis oven was measured to be at around 380 microns in diameter with a large variability due to the nature of the process and diversity of waste tires. The origin of these large agglomerates is mainly the carbonaceous deposits during the pyrolysis decomposition process. To reduce their size, rCB powder was grinded using a Spex/Mixer Mill 8000M with zirconium oxide beads (step A on **Figure 2**).

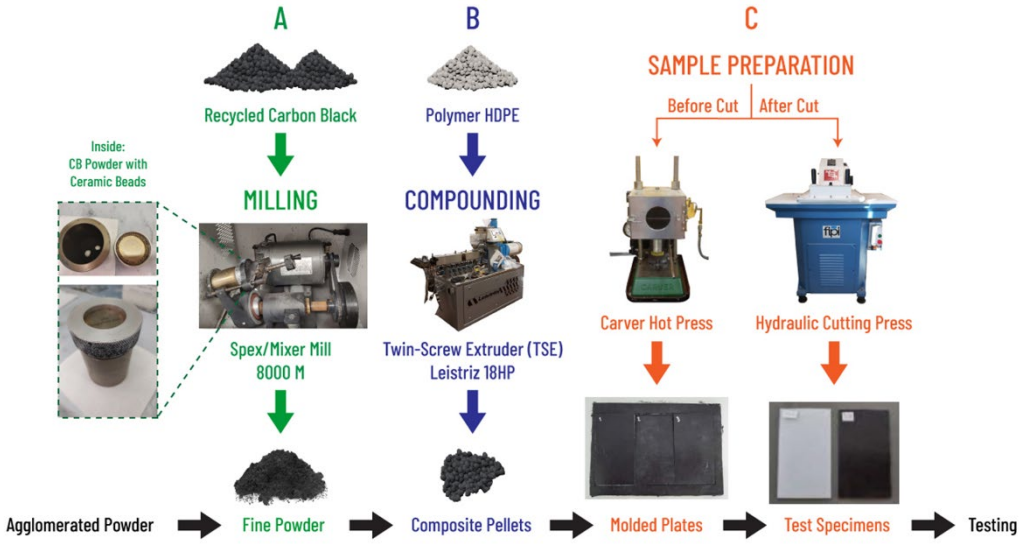

Figure 2. Processing steps for the preparation of composites test specimens.

After milling rCB, the composite material was prepared by mixing the melted polymer with carbon black particles using a twin-screw extruder (step B on **Figure 2**). A Leistriz 18HP twin-screw extruder (TSE) with 8 temperature zones was used with optimized processing conditions for HDPE (see **Figure 3**). HDPE pellets and 6 wt.% of milled rCB were compounded at a temperature varying from 180 to 200°C. Since the virgin HDPE pellets already contain a thermal stabilizer, no additional antioxidant was added to the mix. The extruded filament was pelletized at the exit of the TSW to an average size of 3 mm. To have the same thermal history, the unreinforced HDPE was also prepared using the same processing conditions in the TSE as the composite samples. The manufactured samples are named HDPE for the virgin polymer and R6 for the composite containing 6 wt.% of rCB respectively.

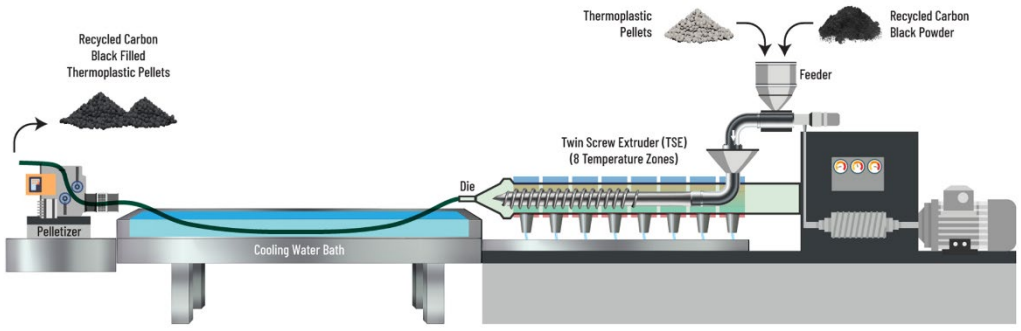

Figure 3. Mixing and extrusion of HDPE/rCB composites with a twin-screw extruder Leistriz 18HP.

Polymer and composite pellets manufactured by TSE were molded into plates of 2 mm thickness using a compression molding technique (step C on **Figure 2**) in a heated hydraulic press (**Figure 4**). A Carver press with plates heated at 170°C and a closing mass of 2 500 kg was used to press mold rectangular flat plates. The molded plates were then cut in 9 cm per 5 cm test specimens using a

 doi:10.20944/preprints202408.1560.v1

hydraulic press and a die cut (step C on **Figure 2**). These samples were used for accelerated aging experiments of this study.

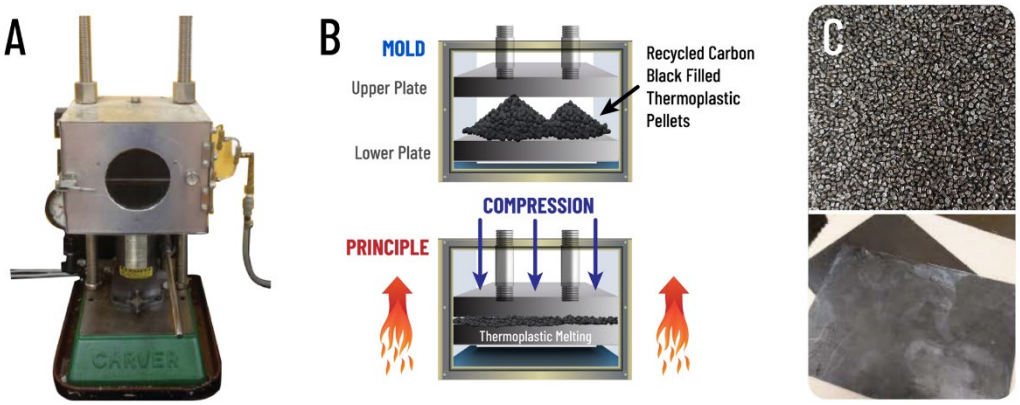

Figure 4. Plate molding: a) Carver hot press, b) mold and molding principle, c) frame containing composite pellets and molded plates.

2.3. Sample Aging

Accelerated aging was carried out in a weathering chamber ARTACC from SEVAR. The samples were placed on the outer part of the moving wheel as illustrated in **Figure 5**. This chamber was built according to ISO 4892-1 standard. The test specimens were held in place with clips and their internal face was exposed to a 400 W medium pressure mercury vapor lamp with an irradiation of 120 W/cm² UVa and 20 W/cm² UVb (EN 60 188 standard requirements). The temperature inside the chamber was 60 ± 0.1°C and water was added in the chamber to simulate natural conditions. The samples undergone six cycles per 24 hours alternating dry and wet cycles, which correspond to 80% of dry irradiation, 5 % of wet irradiation and 15% of wet not irradiated phase. For the non irradiated phase, samples were hidden from the UV lamp by a mask (**Figure 5a**). The exposed face of the sample to UV light was named Fe and the non-exposed face Fne (**Figure 5b**).

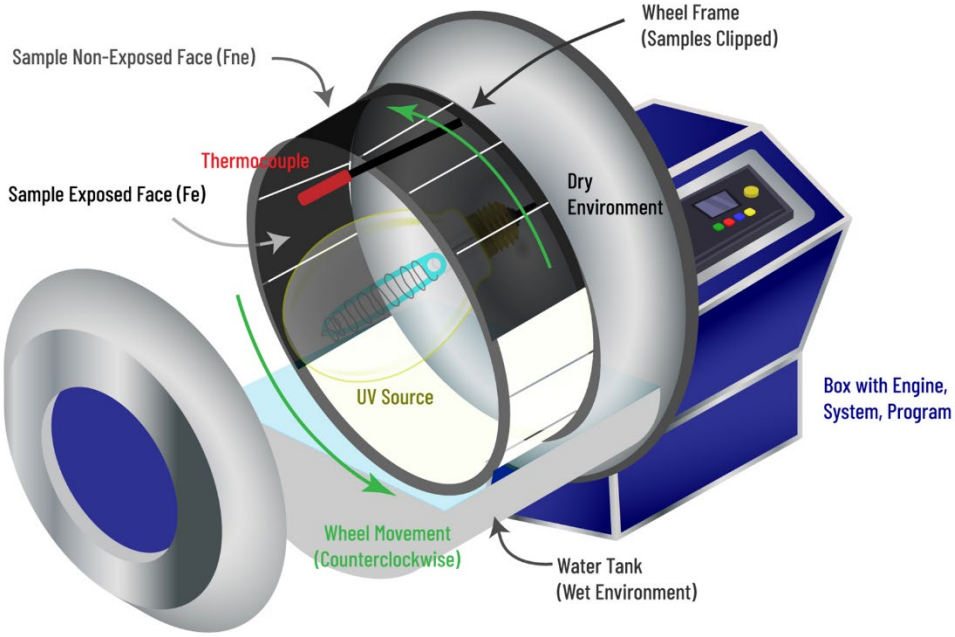

Figure 5. Artacc Bandol Wheel diagram: a) overview of samples placement, b) sample placement indicated exposed and non-exposed faces.

 doi:10.20944/preprints202408.1560.v1

2.4. Sample Analyses

The particle size volume repartition of the recycled carbon black was measured using laser diffraction with a Coulter LS analyzer according to ASTM B822-20 standard. The morphology of the recycled carbon black particles was visualized by high resolution transmission microscopy (HR-TEM) using JEM-21000F/HR 200 kV from JEOL. Energy dispersive X-ray spectroscopy (EDS-X) was performed on the milled particles to verify their composition using field emission environmental scanning electron microscope (ESEM-FEI Quanta 250).

The topography of the surface of the polymer and composite plate samples was studied using a Zeiss Axioskop 2 optical microscope. Particular attention has been paid to the occurrence of cracks during aging. For this purpose, a computer program was developed using Python software which made it possible to quantify the surface changes during aging. Image analysis was performed based on grayscale differences and 3 measurements were carried out per face in order to have an overall representation of the sample.

Chemical degradation of the samples and track of the oxidation products was monitored using a Fourier transformed infrared spectroscopy (FTIR)[21,24,29] with a Perkin Elmer Spectrum Two spectrometer. The FTIR measurements were performed in Attenuated Total Reflectance (ATR) mode, with a range of 4000-500 cm^{-1} wave numbers and a resolution of 4 cm^{-1}. To improve the signal, each spectrum corresponds to 64 accumulations. The FTIR measurements were performed on the exposed and the nonexposed faces with 3 measurements per face to study the homogeneity of the surface oxidation. In all cases, to avoid having edge effects, the measurements were taken more than 10 mm from the edges of the plates. The absorption ATR spectra were processed using OriginPro 2020 from OriginLab analysis software.

For the through-thickness oxidation profiles, the samples were gradually polished using 1000 grade sandpaper. FTIR measurements were performed at each decrease in thickness and were associated with the new thickness resulting from polishing. The polishing was carried out from both the Fe and Fne faces. The material removal was measured using optical microscopy and measurement tools of the microscope software.

3. Results and Discussion

3.1. Carbon Black Analyses

The average diameter of rCB particles from pyrolysis is too large to be directly processed into a thermoplastic resin. Large agglomerates >500 microns are observed and most probably linked to residual carbonaceous deposits from the process which promote the agglomeration of the particles. Carbonaceous deposits are the result of thermal cracking in the pyrolysis oven, they are hard as contain a high amount of carbon, and shear forces generated during the extrusion process are not sufficient to deagglomerate the particles. A secondary upstream process is needed to reduce the size of the agglomerates before they can be incorporated into the polymer resin. Size reduction was carried out using a ball mixer with zirconium oxide balls in dry conditions. **Figure 6** illustrates the volumetric ratio of the powder distribution of the rCB before and after milling and the cumulative percentage. A shift in the average particle size toward lower sizes is observed at more than 1 order of magnitude. The mean size of the agglomerates is reduced by 94% from 380 to 20 microns. The milled rCB also shows more than 20% of particles whose size is less than 10 microns which is expected to improve mechanical performance of the composite.

 doi:10.20944/preprints202408.1560.v1

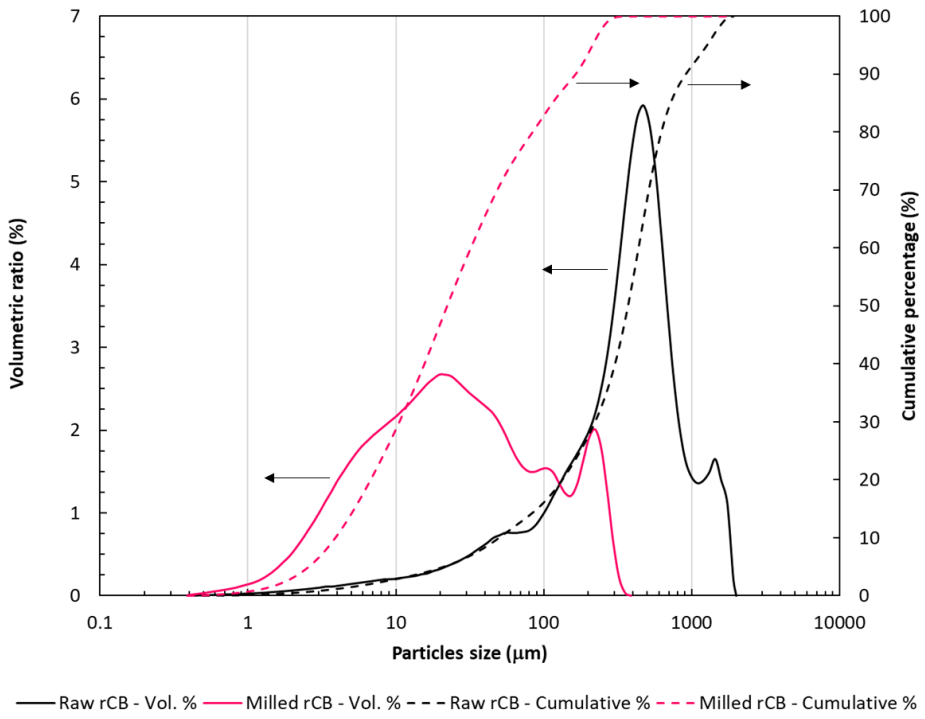

Figure 6. Volumetric ratio of powder distribution (line) and cumulative percentage (dash) of recycled carbon black (rCB) before (black) and after (red) ball milling.

Energy Dispersive X-ray spectroscopy (EDS-X) analyses were performed on rCB particles (**Figure 7**) to verify the composition of the particles and whether there may have been contaminated by the zirconium oxide beads. The rCB shows that it contains mainly elemental carbon, oxygen, and the remaining solid residues from the pyrolysis process that enters the original waste tires composition. The solid additives based on the total remaining residues (removing oxygen and carbon), contain an atomic percentage of 27 ± 3% for silicium, 35 ± 1 % for sulfur, 31 ± 3 % for zinc and 6 ± 1 % for calcium. The EDS-X analysis reveals no significant contamination by the zirconium oxide $ZrO_2(Y_3O_3)$ ceramic beads during the milling process. Thus, grinding should not make any changes other than size reduction of the agglomerates.

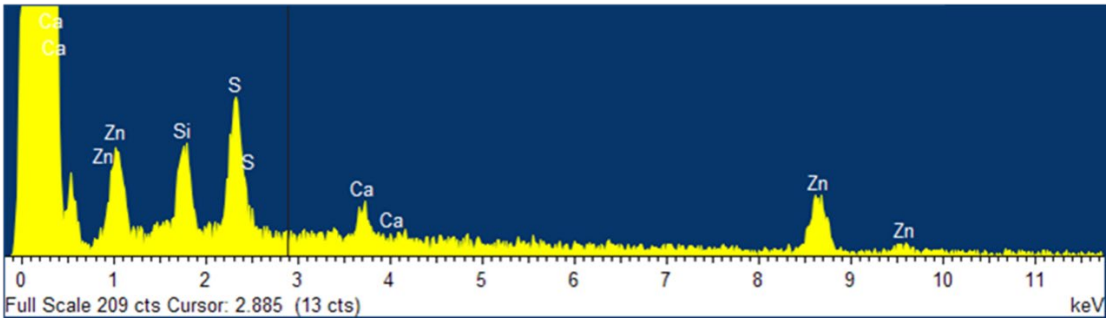

Figure 7. Typical spectrum ESEM EDS-X analysis on rCB particulates.

An additional verification was carried out to for the morphology of the carbon black particles. This has been investigated using HR-TEM as illustrated in **Figure 8**. The milled rCB particles (**Figure 8b**) were compared to a typical commercial carbon black grade used for automotive tire tread, the ASTM N330 (**Figure 8a**). As illustrated, the two types of particles are very similar, both showing stacked graphitic layers in concentric circles, a structure typical of carbon black [30–33].

 doi:10.20944/preprints202408.1560.v1

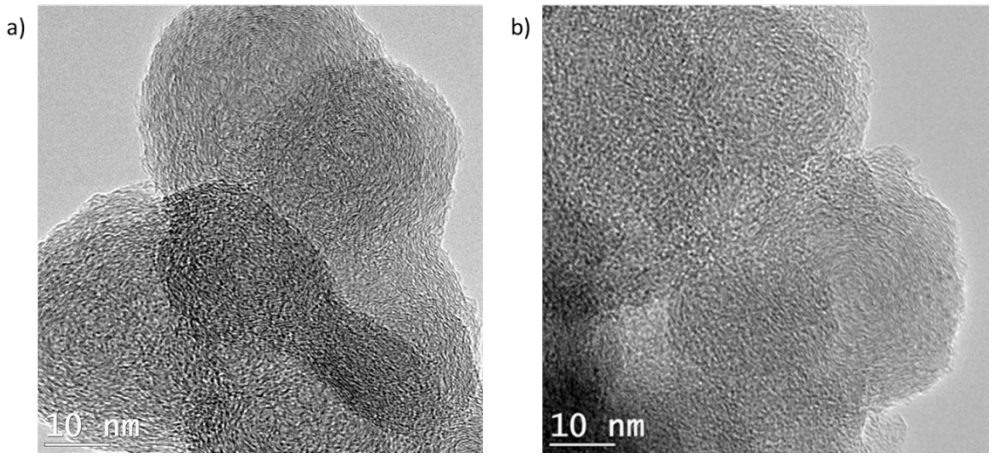

Figure 8. HR-TEM image: a) N330 commercial carbon black used for automotive tire treads, b) recycled carbon black.

3.2. Evolution of Sample Topography with Ageing

The virgin polymer resin HDPE and the composite R6 samples were taken periodically out of the aging chamber and their surface appearance was observed by optical microscopy. **Figure 9** and **Figure 10** show the optical micrographs recorded respectively on HDPE and R6 exposed and non exposed surfaces at different aging times, up to 114 days. The non-exposed (Fne) and exposed (Fe) faces are presented in the left and right columns respectively for comparison.

The virgin HDPE (**Figure 9**), shows that the exposed face starts to crack at 22 days whereas the non-exposed face shows cracks at 36 days of aging. The cracks on Fe at 36 days of aging appear much larger than on Fne. At 64 days, the network of cracks is largely visible and even worse after 114 days of UV exposure. Similar observations were made for polypropylene-polyethylene copolymer exposed to UV accelerated aging conditions in a study by Pertin [34]. Crack propagation is indeed the dominant mechanism of polymer degradation under UV radiation [35,36].

The HDPE/rCB samples R6 show the non exposed face Fne remains unchanged over time with no signs of cracks, even at 114 days of aging as illustrated in **Figure 10**. For the R6 exposed face Fe, cracks start to appear after 64 days of UV exposure and are largely visible after 114 days. Furthermore, cracks do not propagate in the R6 composite the same way they do in virgin HDPE: in HDPE, cracking is significantly important resulting in macro cracks propagating into micro cracks, which is not the case for R6 where only macro cracks are observed on the surface. This highlights the role of carbon black in filtering UV and consequently reducing polymer degradation and crack propagation.

In order to quantify the crack density, image analysis was carried out using Python software. **Figure 11** illustrates the evolution of the surface percentage of cracks during aging for HDPE and R6 samples. Each surface ratio is the average of 3 representative images and the error bars is the associated standard deviation. Hence, the calculation considers the differences in surface homogeneity. The results confirm the microscopy observations. For HDPE, the surface ratio of cracks evolution with aging time is similar for both Fe and Fne surfaces, the cracks density being slightly higher on the exposed face. From 30 days of aging, the crack ratio increases almost linearity with time, reaching 20 % at 114 days of UV exposition for Fe surface. Such a percentage reflects a strong degradation of the surface of the sample. For the Fne surface, the same trend is observed with a slightly lower percentage of cracking which reaches a value of 13 % at 114 days of aging. For R6-Fe, the surface ratio of cracking is significantly lower, not exceeding 5 % at 114 days of aging.

The standard deviation of the measurements reflects the inhomogeneity of the surfaces of the aged samples. For HDPE-Fe, this standard deviation is low at the beginning because the surface only

 doi:10.20944/preprints202408.1560.v1

starts to weakly crack, evenly on the plate. Thereafter, it becomes important because the cracking develops mainly in the center of the plate. At 114 days of aging, the surface is completely covered with cracks, which results in a low standard deviation. This is not the case for the Fne side, which is not yet totally degraded. In the case of R6-Fe, the appearance of cracks remains inhomogeneous and concentrated in the center of the sample, which results in a significant standard deviation.

The apparition of cracks in probably due to a gradient of elasticity in the sample thickness which is shown by a variation in the Young's modulus value as reported by Pertin et al. [37]. During artificial aging, samples undergo thermal expansion and mechanical stresses are build-up on the UV exposed layer and probably released by the occurrence of cracks [37–39].

 doi:10.20944/preprints202408.1560.v1

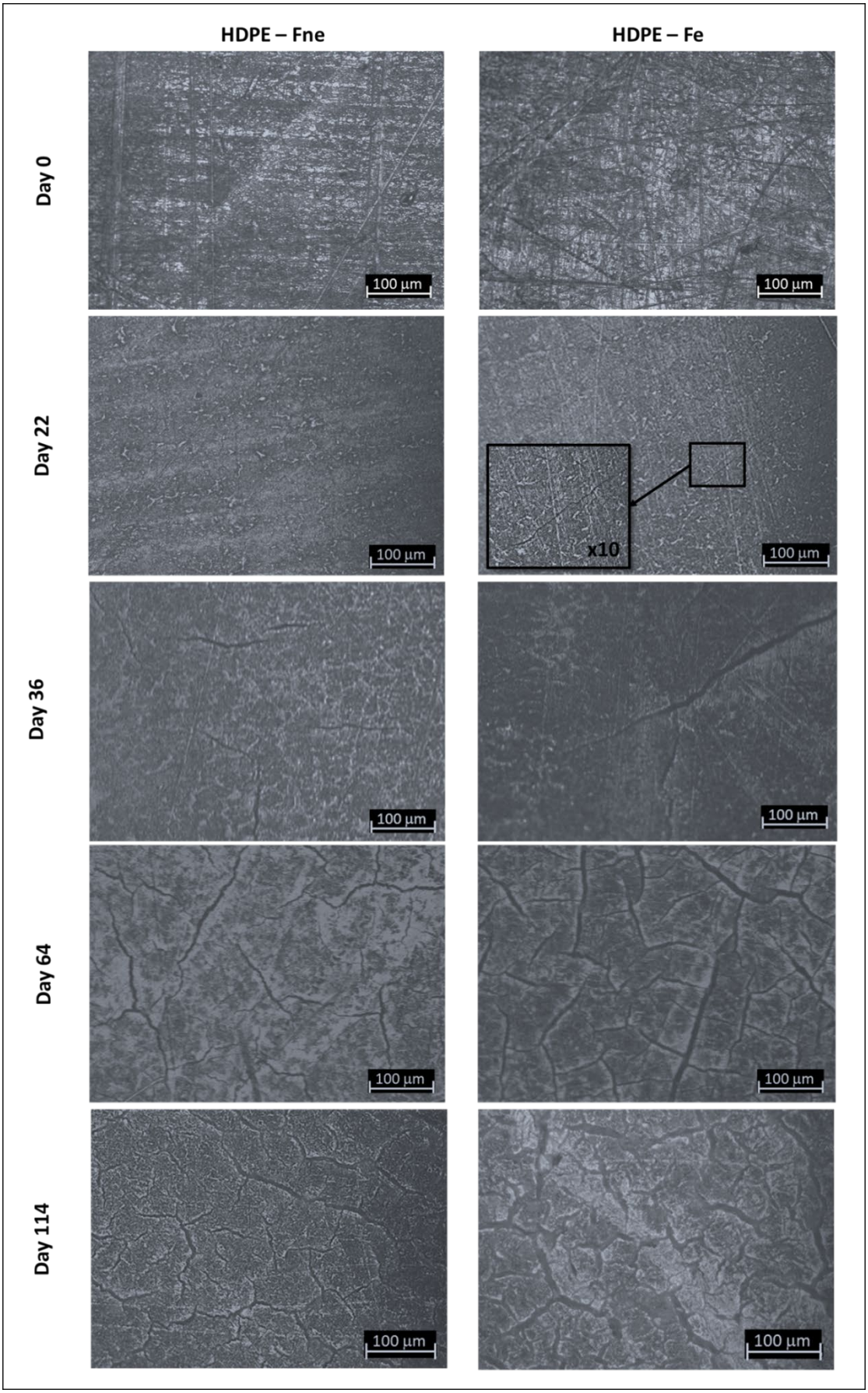

Figure 9. Optical microscopy images of HDPE samples at different aging times.

 doi:10.20944/preprints202408.1560.v1

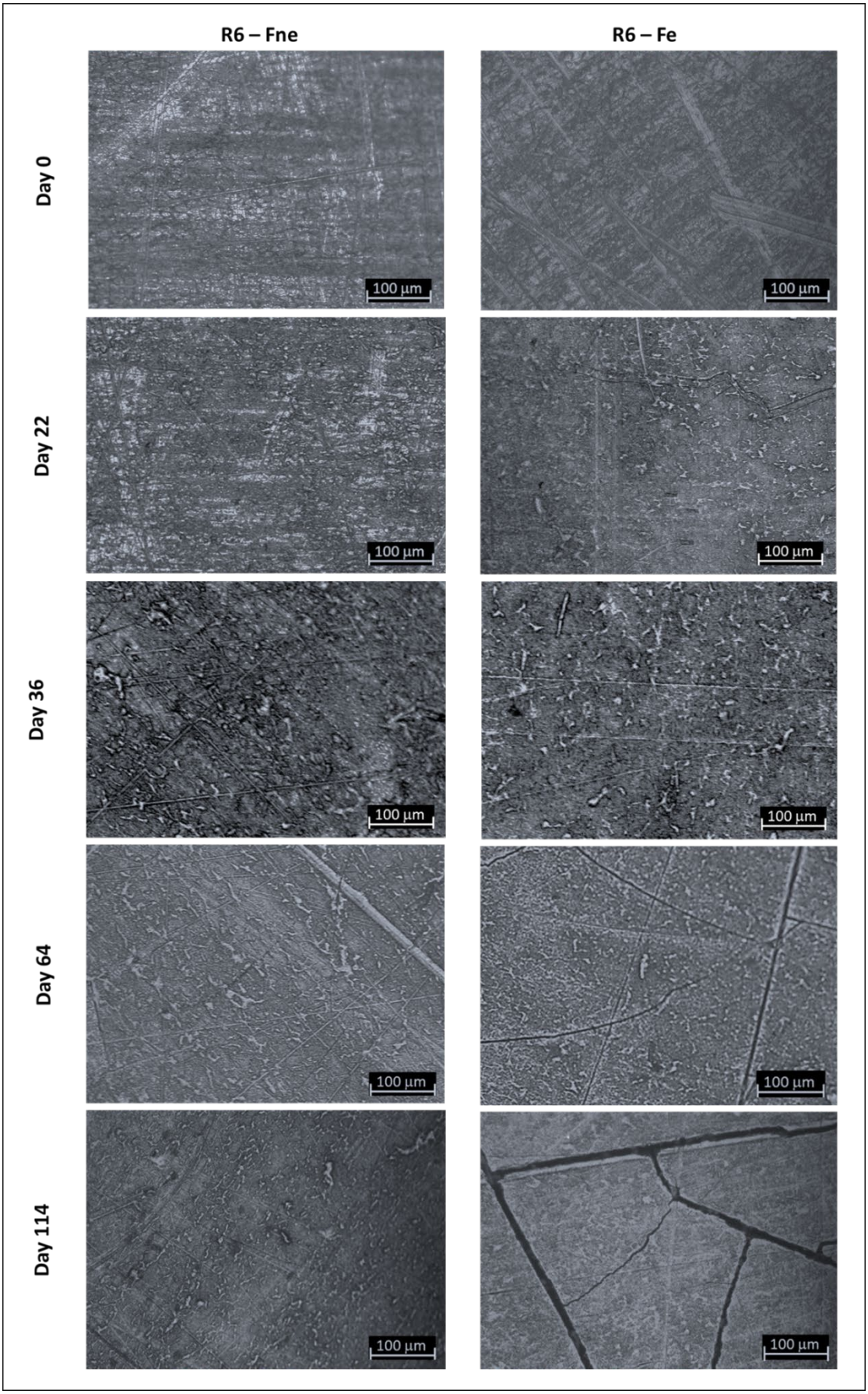

Figure 10. Optical microscopy images of R6 samples at different aging times.

 doi:10.20944/preprints202408.1560.v1

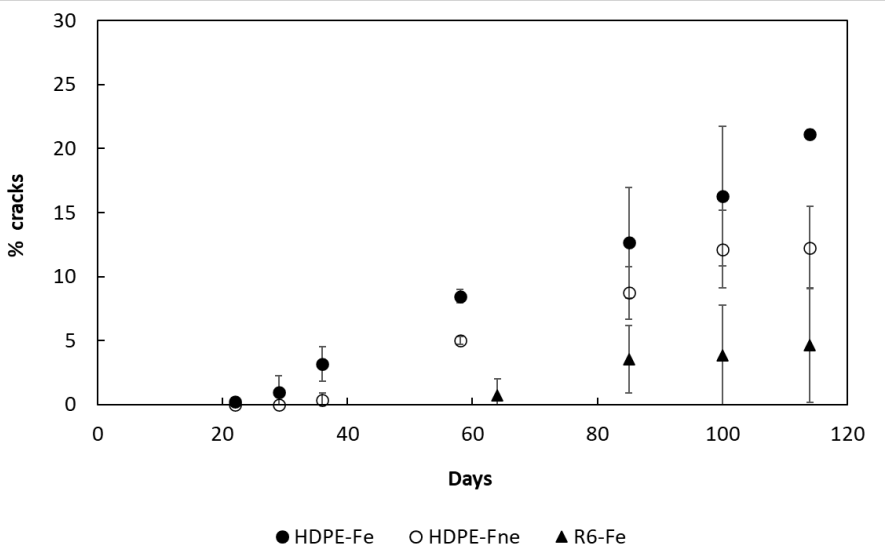

Figure 11. Evolution of the average surface percentage of cracks during photooxidation for HDPE and R6.

3.3. Degradation Kinetic and Formation of Oxidative Products

A typical FTIR spectrum of an 85 days aged HDPE is shown in **Figure 12a**. Three main regions are connected to the oxidation process: the C=C bands (700cm^{-1} to 1300 cm^{-1}) the C=O bands (1500cm^{-1} to 1850 cm^{-1}) and the O-H bands (3200cm^{-1} to 3600 cm^{-1}). **Table 1** summarizes the FTIR absorption spectrum of the HDPE and its main oxidation products usually reported in literature [24,29,40–43]. In this work we have focused on the C=O bands region only, which is the band were the oxidation first appears in HDPE [24,29] and remains predominant in this work. An enlarged view of the carbonyl oxidized region between 1500-1850 cm^{-1} wavelength is illustrated in **Figure 12b**. The band deconvolution shows three mains peaks: carboxylic acid/ketone around 1715 cm^{-1}, γ-lactone at 1780 cm^{-1} and vinyl at 1640 cm^{-1}. These peaks are characteristic of HDPE polymer oxidation products and the cumulative band (red curve) fit well the experimental data (black curve). The carbonyl region is the most apparent for both the virgin HDPE and composite R6 and more specifically the band C=O at 1715 cm^{-1}. The other absorption bands are less well defined, especially for R6, where they are sometimes even confused in the baseline. The baseline indeed presents variations in absorbance of 0.0076 unity of absorbance (u.a.) in the initial FTIR spectra of both HDPE and R6 inside de carbonyl region (1500-1850 cm^{-1}). Absorbance bands below this value are therefore considered as signal noise. Oxidation was quantitatively analysed using the carbonyl index (CI) using the SAUB method [44] and defined as:

$$CI = \frac{Area\ under\ band\ at\ 1715\ cm^{-1}}{Area\ under\ band\ at\ 2912\ cm^{-1}} \quad (1)$$

It is the ratio between the area under the absorbance of C=O at 1715 cm^{-1} and the area of the methylene stretching peak at 2912 cm^{-1}. This latter was chosen as the reference band because it is not altered during aging [40].

 doi:10.20944/preprints202408.1560.v1

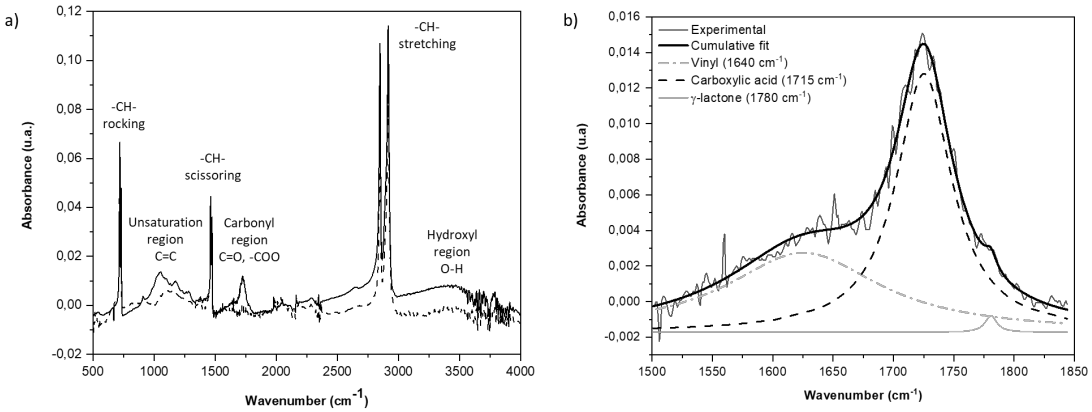

Figure 12. IR spectra of weathered HDPE sample at 85 days: a) global experimental curve of aged (black line) and non aged (black dash) samples and b) zoom on the carbonyl region of the aged sample and peak deconvolution: experimental curve (black line), cumulative fit (thick black line), vinyl (gray dash dot), carboxylic acid / ketone (black dash), γ-lactone (gray line).

Table 1. Spectral FTIR bands studied for HDPE.

Wavenumber [cm^{-1}]	Functionnal groups	
HDPE initial bands		
720	C-H rocking, amorphous	CH_2
730	C-H rocking, crystalline	CH_2
1464	C-H scissoring, amorphous	CH_2
1474	C-H scissoring, crystalline	CH_2
2846	symmetric C-H stretching	CH_2
2912	assymmetric C-H stretching	CH_2
Unsaturation region		
888	Vinylidene	$CH_2=CR_2$
909	Vinyl (C=C-H out of plane bending)	$CH_2=CHR$
965	Vinylene (C=C-H bending)	(Trans) R-CH=CH-R'
Carbonyl region		
1640	Vinyl (C=C vibration)	C=C
1695	Conjugated ketone	$CH_2=CH-CO-CH_3$
1715	Carboxylic acid	R-COO
1720	Ketone	R-C=O-R'
1740	Ester	$R-COO-CH_2$
1760	Peracid	R-COO-OH
1780	γ-Lactone	$(CR_2)_nCO-O$
Hydroxyl region		
3400	Hydroperoxide + alcohol groups	R-COOH-R

Figure 13 illustrates the evolution of CI of virgin HDPE (**Figure 13a**) and composite R6 (**Figure 13b**) of the exposed face (plain symbol) and non exposed face (open symbol) for a maximum aging time of 114 days. The CI was calculated using equation (1). The data shown are the results of the average of 3 measurements for each of the faces and the error bars represent the associated standard deviation. The evolution of the CI of Fe and Fne of HDPE is very similar (**Figure 13a**). Initially, the CI values of Fe and Fne are overlapped below 20 days, then differ slightly. The CI of the Fe faces starts to be higher than that of the Fne faces, after 30 days of aging although differences are very close to error bars. The induction period is less than 10 days, and the CI reaches a saturation plateau value of

 doi:10.20944/preprints202408.1560.v1

30 after 60 days of exposure on both faces. Since ATR analyses is a surface measurement, the saturation observed indicates that the surface layer analysed are fully oxidized.

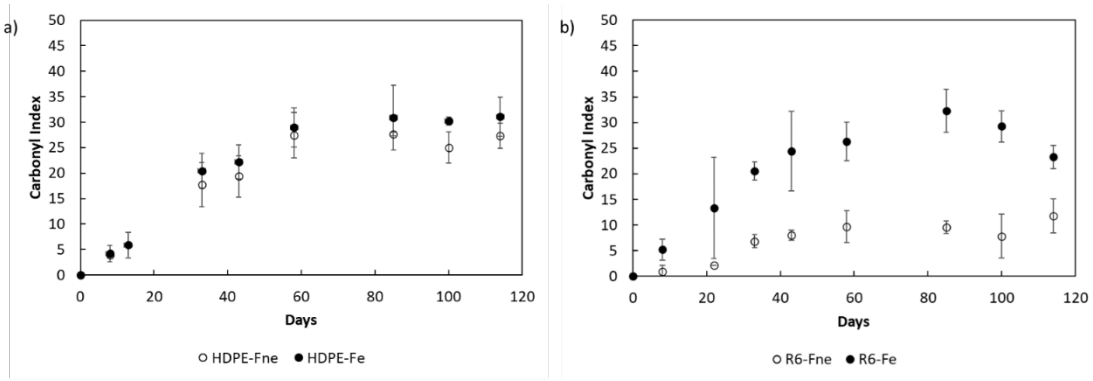

Figure 13. Evolution of the carbonyl index with aging time for a) HDPE b) R6. Open symbols are for the non-exposed face and plain symbols are for the exposed face.

CI measured on the Fe faces of R6 samples show similar behavior than that of the HDPE Fe faces, as illustrated in **Figure 13b**. The induction period is less than 10 days, and a Cl maximum value of 30 occurs at 60 days. Up to 100 days of ageing, the Cl values are identical to those measured on the Fe face of HDPE, considering the errors bars. A slight decrease is observed for aging times greater than 100 days as a Cl value of 24 is measured at 114 days of aging. The reason of this small Cl reduction value is under investigation. The quasi identical results obtained on Fe face of HDPE and R6 samples indicated no significant influence of the rCB particles on the oxidation process of the UV-exposed faces. On the other hand, a quite different behavior is observed for the Fne face of R6 samples. The induction period is longer, close to 20 days (instead of 10 days), and the CI values are significantly lower than those on the Fe face. The saturation value is below 10. This result clearly indicates that the recycled carbon black plays a key role in the antioxidant process for the bulk.

To investigate the oxidation beyond the surface, analyzes were carried out through the thickness of HDPE and the R6 composite samples. For this purpose, the samples were gradually polished and measured for each thickness in FTIR spectroscopy. The CI was calculated using equation (1). **Figure 14** presents the evolution of the carbonyl concentration through the thickness of HDPE and R6 at 114 days of aging. The surface directly exposed to UV light, Fe, is referred to 0 mm depth and the non exposed surface Fne to 2 mm depth. The oxidation profiles measured on both samples are U-type curves as already observed for thick polyethylene [22] and polyolefins [34,45]. The experimental data of the oxidation profiles have been fitted using an exponential curve of the Beer-Lambert law as already reported in other works [37,46]. The following formula was used:

$$CI(x) = A\exp(-x/B) \quad (2)$$

With x is the sample thickness, A is the Cl value at the surface and B is the characteristic depth of the oxidation profile. The corresponding fitting curves are shown in **Figure 14**, with the blue curve for HDPE and the red one for R6. The values of A and B calculated for the Fe and Fne faces of HDPE and R6 samples are reported in **Table 2**. The HDPE curves are quasi symmetrical for Fe and Fne and the characteristic depths of oxidation are similar (162 ± 33 µm for Fe compared to 146 ± 19 µm for Fne).

 doi:10.20944/preprints202408.1560.v1

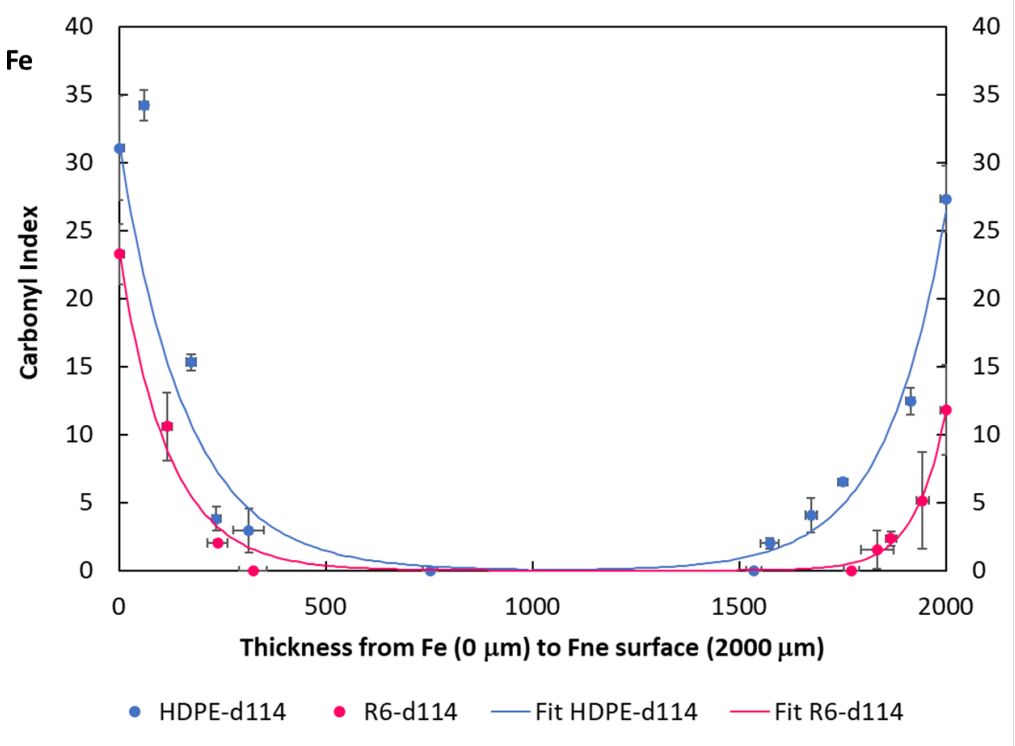

Figure 14. Evolution of the carbonyl concentration through thickness from the exposed face (Fe) to the non-exposed face (Fne).

Table 2. Parameters of the carbonyl index distribution with the thickness for HDPE and R6 at 114 days of aging using an exponential fit.

Material	Face	Coefficient	Value		R^2
HDPE	Fe	A	32 ± 3		0.926
		B	162 ± 34	µm	
	Fne	A	26 ± 2		0.971
		B	147 ± 19	µm	
R6	Fe	A	24 ± 2		0.970
		B	120 ± 20	µm	
	Fne	A	11.7 ± 0.4		0.990
		B	74 ± 6	µm	

For R6 sample the Fne and Fe profiles are asymmetric, the Cl measured for the non-exposed face Fne is 50% lower than that of the Fe face. The depth of the oxide layer close to the Fne-R6 face is also significantly smaller (B =74 ± 6 µm) compared to the Fe-R6 face (B = 120 ± 20 µm). Note that the A and B profile parameters for Fe-R6 are quite similar to those measured on Fe-HDPE sample, although slightly lower. These results highlight that the carbon black particles issued from tires recycling do not have prooxidative action and that, on the contrary, have a totally opposite behavior and act like an antioxidant.

It is well-known that oxidation process is associated to two combined mechanisms: formation of free radical induced by UV absorption and presence of oxygen [36,42]. The quasi symmetric profile observed for HDPE clearly indicates that the photon flux passes through the sample without being significantly absorbed: the quantity of photon being identical on both faces and so the supply of oxygen; the oxidation process is similar. The decrease of Cl value with depth observed for HDPE samples is clearly related to the non ability of oxygen to diffuse into the bulk of the polymer [22,45].

 doi:10.20944/preprints202408.1560.v1

Figure 15a schematically summarizes the symmetric oxygen diffusion profile (black curve), the photon propagation profile (blue dashed line) and the resulting Cl profile (blue line) for HDPE.

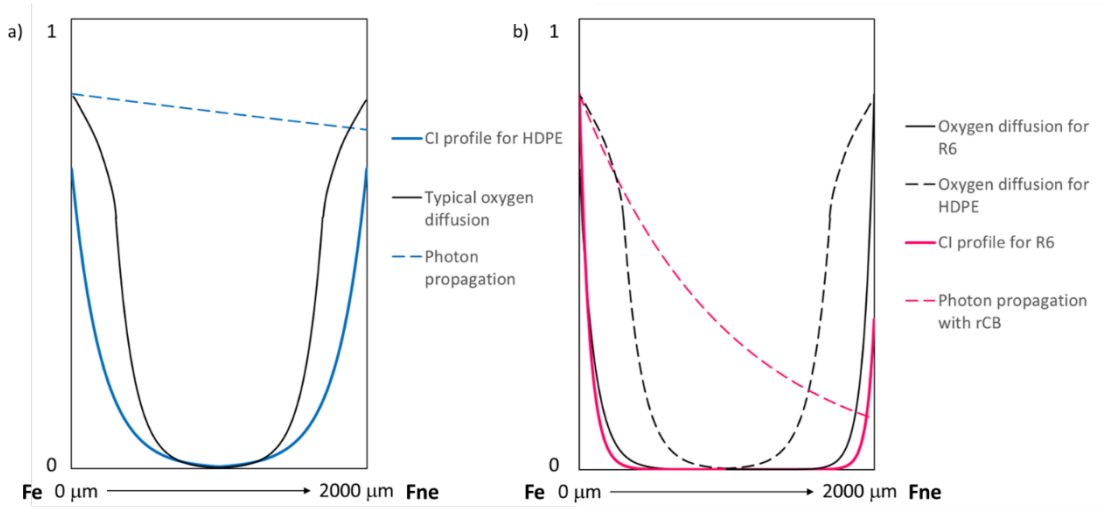

Figure 15. Diagram of the evolution of the oxygen diffusion and the photon propagation and CI through thickness for a) virgin HDPE and b) R6 composite.

Since the oxygen supply is identical for both Fe and Fne faces of the sample, the lower carbonyl index measured on the surface of R6-Fne is clearly related to a lower flux of photons reaching the Fne face due to UV absorption through the thickness of the R6 sample (red dashed-line reported in **Figure 15b**). This result confirms the role of rCB as photon absorber. There is also a significant difference in the characteristic depth of the oxide layer of the Fne and Fe faces (11.7 ± 0.4 µm for Fne-R6 and 24 ± 2 µm for Fe-R6), which suggest that the rCB also affect the diffusion of oxygen into the R6 sample. Also, the surface cracks density (see **Figure 11**) has certainly an influence on the oxidation depth (B parameter). The presence of cracks on the surface of the sample allows the infiltration of the free oxygen, which leads to a higher oxidation depth. This explains the higher B values of Fe-HDPE, Fne-HDPE and Fe-R6 compared to Fne-R6, where no cracks were observed on the sample surface.

In fact, if the oxygen profile was identical for HDPE and R6 samples (black dashed line in **Figure 15b**), the characteristic oxidation depths would be expected to be identical since photons pass through the total thickness for both samples. In order to explain the lower characteristic depth observed for R6 samples, we suggest that the oxygen diffusion is also limited by the presence of rCB particles: the carbon black would also act as a radical scavenger, preventing the radical propagation and thus the oxidation process [12,27]. In the first layers close to the surface, the polymer would be weakly protected against photo-oxidation by the addition of the recycled carbon black alone. However, in the deeper layers, the carbon black, which acts as a UV and oxygen filter, becomes more effective as an oxidation protector. The present work clearly demonstrates that the carbon black issued from waste tires pyrolysis is a promising antioxidating agent.

4. Conclusions

The general goal of this research is to develop a new composite material using a recycled carbon black (rCB) from waste tires to reinforce HDPE. At first, an optimization of the recycled carbon black particles was conducted to deagglomerate the carbonaceous deposits. Grinding of the recycled carbon black particles has allowed to reduce their size close the nanoscale, which made it easier to disperse them in the HDPE polymer. Good quality composite pellets were obtained by mixing/extrusion process in a twin-screw extruder. The performance of the rCB as a filler for UV protection of HDPE was demonstrated by accelerating aging test using and ARTACC environmental chamber. Surface topography analysis of the face exposed to UV radiation of the composite R6 has shown much less cracking than the virgin HDPE polymer (cracks appearing 42 days later). HDPE

 doi:10.20944/preprints202408.1560.v1

has shown macro and micro-cracking on both faces (Fe and Fne) whereas for R6 samples the exposed face shows only macro-cracking and the non exposed face remains unchanged. This highlights the role of rCB in preventing the propagation of cracks in the polymer.

The FTIR results have shown that the rCB added to the polymer has not only an absorption protective action against UV radiation but probably play a significant role in oxygen diffusion through the sample. The composite R6 shows less surface oxidation (CI 24% less for Fe surface) than the virgin HDPE and the photons penetrate less through the sample thickness (CI reduced by 54% for Fne surface). The oxidation profile of the composite is also different between the two surfaces of the exposed and non exposed faces, as opposed to HDPE where they are nearly identical. This illustrates the absorption role of rCB, hindered the penetration of photons. The oxidation in the sample bulk is reduced by more than half for R6 in comparison to HDPE (120 µm from Fe and 74 µm from Fne, for R6).

This study has demonstrated that the recycled carbon black resulting from waste tires vacuum pyrolysis is a promising approach to revalorize tire waste with an eco-responsible processing. The use of rCB as filler for HDPE used for outdoor applications has demonstrated to be an antioxidant for UV protection and good substitute for commercial carbon black for industrial goods. In the ecological perspective, the vacuum pyrolysis process used in this study can be easily implantable in limited access areas as the Guadeloupe island to overcome the ecological devastating reality of waste tires land fields. Current studies focus on improving recycled black by surface modifications to improve functionalization, adhesion to the polymer matrix and reduce aging.

Acknowledgments: The authors acknowledge the support of the industrial partner Pyrovac Inc., Saint-Lambert de Lauzon (Québec, Canada), for supporting this research project and the supply of the recycled carbon black. The financial contribution of the National Sciences and Engineering Research Council of Canada (NSERC), INNOV-R and Prima Québec, is also greatly appreciated.

References

1. M. Sienkiewicz, J. Kucinska-Lipka, H. Janik, and A. Balas, "Progress is used types management in the European Union: A review," *Waste Management*, vol. 32, pp. 1742-1751, 2012.
2. A. T. Hoang, T. H. Nguyen, and H. P. Nguyen, "Scrap tire pyrolysis as a potential stategy for waste management pathway: a review," *Energy Sources, Part A: Recovery, Utilization, and Environmental Effects*, 2020.
3. J. D. Martinez, N. Puy, R. Murillo, T. Garcia, M. V. Navarro, and A. M. Mastral, "Waste tyre pyrolysis - A review," *Renewable and Sustainable Energy Reviews*, vol. 23, pp. 179-213, 2013.
4. ADEME, "Pneumatiques - Données 2020," ADEME, Angers (France)2020.
5. ACARP, "Rapport annuel 2021 de l'Association Canadienne des Agences de Recyclage des Pneus," 2021.
6. USTMA, "2019 US Scrapt Tire Management Summary," 2019.
7. J. Xu, J. Yu, J. Xu, C. Sun, W. He, J. huang, and G. Li, "High-value utilization of waste tires: A review with focus on modified carbon black from pyrolysis," *Science of the Total Environment*, vol. 742, 2020.
8. P. T. Williams, "Pyrolysis of waste tyres: a review," *Waste Management*, vol. 33, pp. 1714-1728, 2013.
9. C. Roy, A. Chaala, H. Darmstadt, B. de Caumia, H. Pakdel, and J. Yang, "Conversion of used tires to carbon black and oil by pyrolysis," in *Rubber Recycling*, ed: CRC Press, Taylor & Francis Group, LLC., 2005, p. 528.
10. S. Deveci, N. Antony, and B. Eryigit, "Effect of carbon black distribution on the properties of polyethylene pipes - Part 1: Degradation of post yield mechanical properties and fracture surface analyses," *Polymer Degradation and Stability*, vol. 148, pp. 75-85, 2018.
11. V. T. Wallder, W. J. Clarke, J. B. Decoste, and J. B. Howard, "Weathering Studies on Polyethylene," *Industrial & Engineering Chemistry*, vol. 42, pp. 2320-2325, 1950.
12. A. R. Horrocks, J. Mwila, M. Miraftab, M. Liu, and S. S. Chohan, "The influence of carbon black on properties of orientated polypropylene 2. Thermal and photodegradation," *Polymer Degradation and Stability*, vol. 65, pp. 25-36, 1999.
13. E. L. Crump, "Economic Impact Analysis For the Proposed Carbon Black Manufacturing NESHAP," U.S. Environmental Protection Agency (EPA)2000.
14. Ecoinvent. (2019). *ecoinvent v3.6 database*. Available: https://ecoinvent.org
15. C. Roy, B. Labrecque, and B. De Caumia, "Recycling of scrap tires to oil and carbon black by vacuum pyrolysis," *Resources, Conservation and Recycling*, vol. 4, pp. 203-213, 1990.
16. LRCCP, "Bioproof - Rapports axe Recyclage," Vitry-sur-Seine (France)2018.

 doi:10.20944/preprints202408.1560.v1

17. S.-Q. Li, Q. Yao, Y. Chi, J.-H. Yan, and K.-F. Cen, "Pilot-Scale Pyrolysis of Scrap Tires in a Continuous Rotary Kiln Reactor," *Industrial & Engineering Chemistry Research,* vol. 43, pp. 5133-5145, 2004.
18. B. Sahouli, S. Blacher, F. Brouers, H. Darmstadt, C. Roy, and S. Kaliaguine, "Surface morphology and chemistry of commercial carbon black and carbon black from vacuum pyrolysis of used tyres " *Fuel,* vol. 75, pp. 1244-1250, 1996.
19. C. Roy and H. Darmstadt, "Carbon blacks recovered from rubber waste by vacuum pyrolysis - comparison with commercial grades," presented at the International Conference on Rubbers, Calcutta (India), 1998.
20. F. Environmental. (2014, February 2022). *Solar Radiation and Photosynethically Active Radiation*. Available: https://www.fondriest.com/environmental-measurements/parameters/weather/photosynthetically-active-radiation/
21. P. Gijsman, G. Meijers, and G. Vitarelli, "Comparison of the UV-degradation chemistry of polypropylene, polyethylene, polyamide 6 and polybutylene terephthalate," *Polymer Degradation and Stability,* vol. 65, pp. 433-441, 1999.
22. G. C. Furneaux, K. J. Ledbury, and A. Davis, "Photo-oxidation of thick polymer samples - Part 1: the variation of photo-oxidation with depth in naturally and artificially weathered low density polyethylene," *Polymer Degradation and Stability,* vol. 3, pp. 431-442, 1981.
23. F. Tüdos and M. Iring, "Polyolefine oxidation: rates and products," *Acta Polymerica,* vol. 39, pp. 19-26, 1988.
24. M. Gardette, A. Perthue, J.-L. Gardette, T. Janecska, E. Foldes, B. Pukanszky, and S. Therias, "Photo- and thermal-oxidation of polyethylene: Comparison of mechanisms and influence of unsaturation content," *Polymer Degradation and Stability,* vol. 98, pp. 2383-2390, 2013.
25. E. Yousif and R. Haddad, "Photodegradation and photostabilization of polymers, especially polystyrene: a review," *Springer Plus,* vol. 2, pp. 398-430, 2013.
26. J. Mwila, M. Miraftab, and A. R. Horrocks, "Effect of carbon black on the oxidation of polyolefins - An overview," *Polymer Degradation and Stability,* vol. 44, pp. 351-356, 1994.
27. W. L. Hawkins, R. H. Hansen, W. Matreyek, and F. H. Winslow, "The effect of carbon black on thermal antioxidants for polyethylene," *Journal of Applied Polymer Science,* vol. 1, pp. 37-42, 1959.
28. D. Chemicals, "DOW DMDA-8904 NT 7 High Density Polyethylene Resin - Technical Information," Dow Chemicals2018.
29. F. Carrasco, P. Pagès, S. Pascual, and X. Colom, "Artificial aging of high-density polyethylene by ultraviolet irradiation," *European Polymer Journal,* vol. 37, pp. 1457-1464, 2001.
30. J.-B. Donnet, "Structure and Reactivity of Carbon," *Tanso,* vol. 88, pp. 12-33, 1977.
31. K. Ono, M. Yanak, S. Tanaka, Y. Saito, H. Aoki, O. Fukuda, T. Aoki, and T. Yamaguchi, "Influence of furnace temperature and residence time on configurations of carbon blacks," *Chemical Engineering Journal,* vol. 200-202, pp. 541-548, 2012.
32. R. P. J. Hjelm, W. A. Wampler, P. A. Seeger, and M. Gerspacher, "The microstructure and morphology of carbon black: A study using small angle neutron scattering and contrast variation," *Journal of Materials Research,* vol. 9, pp. 3210-3222, 1994.
33. A. I. Medalia, "Morphology of Aggregates - VI. Effective volume of aggregates of carbon black from electron microscopy; application to vehicule absorption and to die swell of filled rubber," *Journal of Colloid and Interface Science,* vol. 22, pp. 115-131, 1970.
34. T. Pertin, "Etude d'une matrice thermoplastique sous contraintes environnementales tropicales : approche multi-échelle," PhD, Physic department, Université des Antilles, Guadeloupe (FWI), 2022.
35. I. Yakimets, D. Lai, and M. Guigon, "Effect of photo-oxidation cracks on behaviour of thick polypropylene samples," *Polymer Degradation and Stability,* vol. 86, pp. 59-67, 2004.
36. M. Liu and A. R. Horrocks, "Effect of Carbon Black on UV stability of LLDPE films under artificial weathering conditions," *Polymer Degradation and Stability,* vol. 75, pp. 485-499, 2002.
37. T. Pertin, G. Minatchy, M. Adoue, A. Flory, and L. Romana, "Investigation of nanoindentation as a fast characterization tool for polymer degradation study," *Polymer Testing,* vol. 81, 2019.
38. R. Yang, Y. Liu, and D. Zhang, "Spatial Heterogeneity of Photo-Oxidation and Its Relation With Crack Propagation in Polyethylene Composites," *Polymer Engineering and Science,* vol. 48, pp. 2270-2276, 2008.
39. R. K. Krishnaswamy, Q. Yang, L. Fernandez-Ballester, and J. A. Kornfield, "Effect of the Distribution of Short-Chain Branches on Crystallization Kinetics and Mechanical Properties of High-Density Polyethylene," *Macromolecules,* vol. 41, pp. 1693-1704, 2008.
40. N. M. Stark and L. M. Matuana, "Surface chemistry changes of weathered HDPE/wood-flour composites studied by XPS and FTIR spectroscopy," *Polymer Degradation and Stability,* vol. 86, pp. 1-9, 2004.
41. A. Tidjani, "Comparison of formation of oxidation products during photo-oxidation of linear low density polyethylene under different natural and accelerated weathering conditions," *Polymer Degradation and Stability,* vol. 68, pp. 465-469, 2000.
42. G. Grause, M.-F. Chien, and C. Inoue, "Changes during the weathering of polyolefins," *Polymer Degradation and Stability,* vol. 181, 2020.

 doi:10.20944/preprints202408.1560.v1

43. L. Douminge, "Étude du comportement du polyéthylène haute densité sous irradiation ultraviolette ou sollicitation mécanique par spectroscopie de fluorescence," Thèse de Doctorat Spécialité Science des Matériaux, UFR Sciences Fondamentales et Sciences pour l'Ingénieur - Science des Matériaux, Université de La Rochelle, La Rochelle (France), 2010.
44. J. Almond, P. Sugumaar, M. N. Wenzel, G. Hill, and C. Wallis, "Determination of the carbonyl index of polyethylene and polypropylene using specified area under band methodology with ATR-FTIR spectroscopy," *e-Polymer*, vol. 20, pp. 369-381, 2020.
45. A. V. Cunliffe and A. Davis, "Photo-oxidation of thick polymer samples - Part II: The influence of oxygen diffusion on the natural and artificial weathering of polyolefins," *Polymer Degradation and Stability*, vol. 4, pp. 17-37, 1982.
46. E. Richaud and J. Verdu, "Vieillissement chimique des polymères - Cinétique de dégradation (AM3152 V1)," in *Technique de l'ingénieur*, T. d. l'ingénieur, Ed., ed France: Technique de l'ingénieur, 2011.